THE JOURNAL OF PHYSICAL CHEMISTRY A

Article

Cite This: J. Phys. Chem. A 2018, 122, 9474−9482

pubs.acs.org/JPCA

# Unique Surface Enhanced Raman Scattering Substrate for the Study of Arsenic Speciation and Detection

Shuyu Xu,[†] Fernando P. Sabino,[†] Anderson Janotti,[†] D. Bruce Chase,[†] Donald L. Sparks,[‡] and John F. Rabolt*[,†]

[†]Department of Materials Science and Engineering and [‡]Department of Plant and Soil Sciences, University of Delaware, Newark, Delaware 19716, United States

Supporting Information

**ABSTRACT:** In this study, a three-dimensional surface enhanced Raman scattering (SERS) substrate comprised of silver coated gold nanorods (Ag/AuNRs) decorated on electrospun polycaprolactone (PCL) fibers has been applied, *for the first time*, to quantitative analytical measurements on various arsenic species: *p*-arsanilic acid (*p*AsA), roxarsone (Rox), and arsenate ($As^V$), with a demonstrated sensitivity below 5 ppb. $As^V$ detection in a solution of common salt ions has been demonstrated, showing the tolerance of the substrate to more complex environments. *p*AsA adsorption behavior on the substrate surface has been investigated in detail using these unique SERS substrates. Calculations based on density functional theory (DFT) support the spectral observation for *p*AsA. This substrate also has been shown to serve as a platform for in situ studies of arsenic desorption and reduction. This SERS substrate is potentially an excellent environmental sensor for both fundamental studies and practical applications.

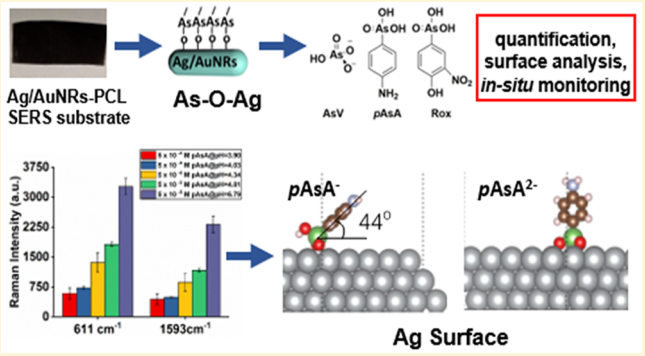


## INTRODUCTION

Arsenic contamination is a worldwide problem with the metalloid found naturally in water, mines, and soils in a variety of forms. Concern with the hazards of arsenic in the environment and exposure to human beings has led the World Health Organization (WHO) to set a stringent standard with a maximum of 10 ppb (μg/L) in drinking water. However, it has been reported that drinking water with arsenic levels at concentrations above the WHO standard has already affected over a million people in 50 countries. This is especially true for developing countries in South Asia (e.g., Bangladesh) and South America (e.g., Chile).[1,2] The long-term exposure to arsenic in food and drinking water increases significantly the risks of carcinogenesis, reproductive problems, and cardiovascular disease.[3,4]

Different forms of arsenic have different toxicities and a variety of uses. Arsenate ($As^V$) and arsenite ($As^{III}$) are inorganic arsenic species and the most dominant forms of arsenic found in water. $As^V$ is the main species found in the aerobic environment, while $As^{III}$ prevails in a more reductive environment and can be 50−100 times more toxic than $As^V$.[5] Organoarsenic compounds, such as *p*-arsanilic acid (*p*AsA) and roxarsone (Rox), are widely used in poultry farming as feed additives to improve feed efficiency and control diseases. The majority of these antimicrobial drugs, however, are not metabolized in poultry, and are excreted chemically unchanged in farming litter. Along with the farming litter used as fertilizer in agricultural planting, these organic arsenic compounds will finally degrade to other organic/inorganic arsenic species, such as $As^V$, $As^{III}$, dimethylarsinic acid (DMA), and monomethylarsonic acid (MMA), with higher mobility and toxicity that accumulate in the soil, underground water, and rice.[6−8]

The toxicity, mobility, and degradation of various arsenic species are known to be closely related to their chemical forms, oxidation states, and valences. Therefore, speciation of arsenic pollution is sometimes much more important than a simple detection of the total amount of arsenic. Many analytical techniques have been developed and are routinely used in analytical laboratories for arsenic detection. These include atomic fluorescence spectroscopy (AFS), atomic absorption spectroscopy (AAS), inductively coupled plasma atomic emission spectrometry or mass spectrometry (ICP-AES or ICP-MS), as well as other wet chemical methods.[9] Although high sensitivity has been reached, most of these techniques only give results for the total arsenic content with no differentiation of arsenic species. Coupled with effective separation methods such as ion chromatography (IC) or high-performance liquid chromatography (HPLC) with a carefully designed column, the above-noted techniques can execute the quantification and speciation of arsenic analysis.[10−12] However, these instrumental techniques are still expensive and bulky, and sample preparation is sophisticated

Received: September 17, 2018
Revised: November 5, 2018
Published: November 12, 2018







DOI: 10.1021/acs.jpca.8b09104
J. Phys. Chem. A 2018, 122, 9474−9482

and time-consuming. This limitation has led to a need for a fast, sensitive, and reproducible analytical method for arsenic analysis.

Surface-enhanced Raman scattering (SERS) has emerged as a promising technique for ultrasensitive arsenic analysis. In recent years, SERS has been extensively used in environmental analysis and monitoring,[13,14] including detection of arsenic in water.[4] Extended X-ray absorption fine structure (EXAFS) analysis has suggested $As^{V}$ is chemically adsorbed onto a silver surface by the formation of As−O−Ag bonds,[15] and the difference in Raman shift (~60 $cm^{-1}$) of As−O stretching between $As^{V}$ and $As^{III}$ helped identify arsenic in different valences.[16] This makes silver-based nanostructures excellent SERS platforms for arsenic detection. Silver colloids of various shapes and modifications have been studied for arsenic detection.[16−18] In addition, silver nanofilms fabricated by mirror reactions[19−21] and two-phase interfacial self-assembly[22] have also been utilized as SERS substrates for arsenic detection. A limit of detection (LOD) of around 1 ppb has been reached for both $As^{V}$[16] and $As^{III}$.[17] However, previous SERS sensors for arsenic detection used either colloidal suspensions or two-dimensional (2D) solid substrates. A three-dimensional (3D) substrate fabricated using metallic nanoparticle (MNPs)/polymer composites has not been reported as a SERS sensor for arsenic analysis. In our previous studies, a protocol for SERS substrate fabrication has been developed using Ag/AuNRs and electrospun polycaprolactone (PCL) fibrous mats with electrostatic binding of Ag/AuNRs to the PCL nanofibers.[23] This 3D SERS substrate has demonstrated high sensitivity and reproducibility, and it provides suitable surface chemistry for arsenic detection. In this work, we have conducted SERS studies directed at arsenic analysis with this substrate. In addition to quantitative SERS measurements of different arsenic species, in situ observations of arsenic activities (i.e., $As^{V}$ desorption) have been carried out. More importantly, by analyzing SERS spectra of *p*AsA at different concentrations and pH values, we have determined the surface adsorption behaviors of *p*AsA tautomers on silver surfaces. Density functional theory (DFT) calculations of *p*AsA tautomers interacting with a silver surface have been carried out to further elucidate the SERS activities of *p*AsA. These studies using SERS exhibit the power and versatility of the SERS technique with our unique 3D Ag/AuNR substrates for arsenic analysis in environmental sensing applications.

## EXPERIMENTAL SECTION

Cetyltrimethylammonium bromide (CTAB) and cetyltrimethylammonium chloride (CTAC) were purchased from TCI, Inc. 3-Nitro-4-hydroxyphenylarsonic acid (roxarsone, Rox) was purchased from Fisher Scientific, and 4-aminophenylarsonic acid (4-arsanilic acid, *p*AsA) was purchased from Alfa Aesar. All the other chemicals were purchased from Sigma-Aldrich. All chemicals were used as received. Deionized (DI) water (18.2 MΩ·cm; Millipore Co.) was used for solution preparations unless otherwise described.

**Fabrication of 3D Ag/AuNR-Based SERS Substrate.** The fabrication of Ag/AuNR−PCL SERS substrate has been given in our previous study.[23] Specifically, 5 nm thick silver layer coated AuNRs with a width of approximately 25 nm and a length of about 70 nm were used as SERS-active MNPs for substrate fabrication and arsenic analysis. This substrate resulted in the optimum SERS performance as discussed in our previous studies.

**Quantitative Measurements of Arsenic Species.** Arsenic solution samples were prepared in various concentrations with identical volumes of 10 mL. A piece of SERS substrate was cut into identical pieces (typically 2 mm × 10 mm). Each piece was immersed into a sample solution containing a different concentration of arsenic for 2 h, and then taken out and washed with DI water to remove loosely bound analyte molecules. The substrates were dried under ambient temperature and humidity before SERS measurements. The measurements were performed using a Kaiser Holospec 1.8 Raman Spectrograph equipped with a TE cooled Andor CCD and an ONDAX 785 nm laser and probe head. The Raman instrument uses an 800 lines/mm transmission holographic grating, and the numerical aperture is 0.9 with a magnification of 65×. For each sample, measurements were recorded on three randomly selected spots on the substrate using ~0.8 mW laser power at the sample with a 10 s exposure for 10 accumulations. To test arsenic detection in a more complex environment, $As^{V}$ solutions containing common salt ions (30 μM $Na^{+}$, 10 μM $K^{+}$, 10 μM $Mg^{2+}$, 10 μM $Ca^{2+}$, 10 μM $Cl^{-}$, 10 μM $HPO_4^{2-}$, 10 μM $SO_4^{2-}$, 20 μM $NO_3^{-}$, 10 μM $H_2PO_4^{-}$) were prepared at different concentrations. The sample preparation and SERS measurements were similar to the procedures described above.

To achieve rigorous data analysis, spectra were processed before plotting in the following sequence: Each spectrum was the average of three measurements. All the spectra were baseline corrected. A background spectrum was then subtracted, and the result was offset to read zero in regions where there were no Raman peaks. The background spectrum was obtained using a bare substrate immersed in a blank solution (DI water or common salt ions solution without arsenic analyte) under the same experimental conditions.

**SERS of *p*AsA at Different pHs.** To explore the effect of pH on the SERS spectra of *p*AsA, $5 \times 10^{-4}$ M *p*AsA solution samples at different pHs were prepared. The pH of a solution was adjusted by adding an appropriate amount of 0.1 M NaOH, and the pH of the resultant solution was measured with a pH Meter (Fisher Scientific, accumet AB15 Basic). The preparation of SERS samples, acquisition of SERS spectra, and data processing followed the previous description.

**In Situ SERS Monitoring of Arsenic Activities.** To conduct in situ SERS measurement, a piece of SERS substrate was immersed in $10^{-4}$ M $As^{V}$ solution for 2 h, washed with DI water, and dried. The substrate was then immersed into 10 mL of 20 mg/L NaCl and $KH_2PO_4$ solution respectively and placed in the Raman instrument for desorption monitoring. Raman spectra were recorded in situ on the same sample spot of the substrate in the solution, with 1 s exposure for 60 accumulations. For in situ reduction of Rox, a piece of SERS substrate was immersed in $5 \times 10^{-5}$ M Rox solution in DI water for 2 h, washed with DI water, and dried. The substrate was then immersed into 2 mM $NaBH_4$ solution for in situ reduction monitoring. Raman acquisition of the Rox reduction was the same as for the $As^{V}$ desorption experiment.

## COMPUTATIONAL APPROACH

First-principles calculations based on DFT[24,25] were performed to explore the possible configurations of *p*AsA on the Ag surface. We used the generalized gradient approximation of Perdew, Burke, and Ernzerhof (PBE)[26] with van der Waals correction as proposed by Grimme,[27,28] which includes two- and three-body terms (D3).[28,29] The projected augmented



DOI: 10.1021/acs.jpca.8b09104
J. Phys. Chem. A 2018, 122, 9474−9482

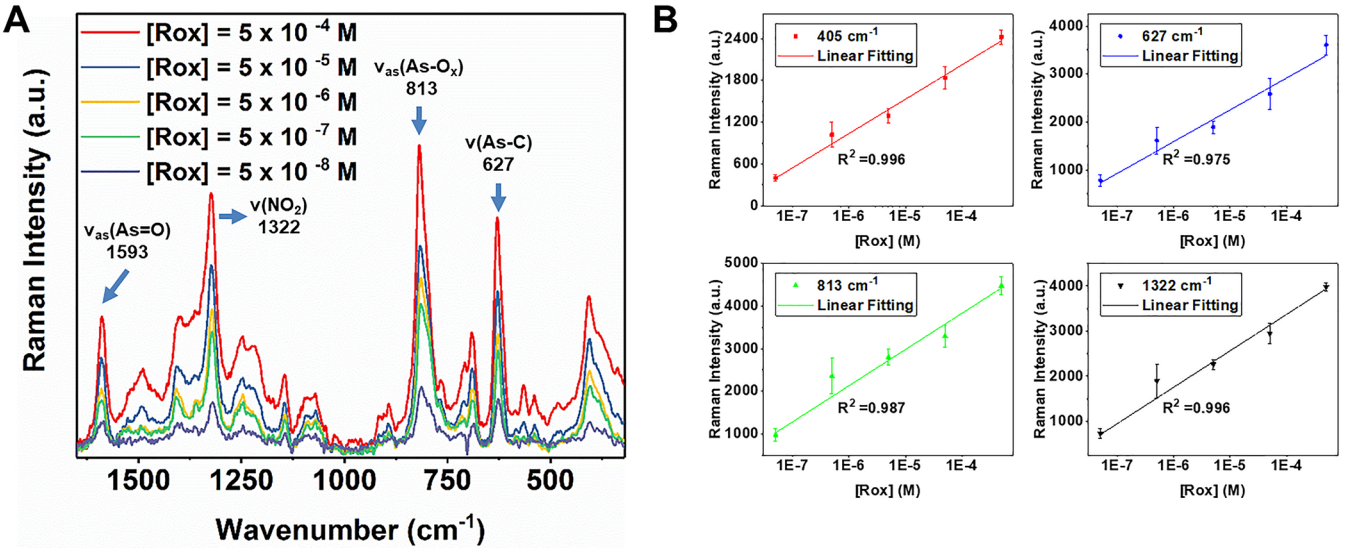


**Figure 1.** (A) SERS spectra of Rox with concentrations ranging from $5 \times 10^{-8}$ to $5 \times 10^{-4}$ M. (B) SERS quantification of Rox against concentration for peaks at 405, 627, 813, and 1322 $cm^{-1}$.

**Table 1. Peak Assignments of *p*AsA and Rox in Normal Raman and SERS Spectra**

| | *p*AsA ($cm^{-1}$) | | | Rox ($cm^{-1}$) | |
|---|---|---|---|---|---|
| assignment[34] | Raman | SERS | assignment[34] | Raman | SERS |
| $\nu$(Ag−O) | | 210 | $\nu$(Ag−O) | | 229 |
| 16a(a′) | | 400 | $\gamma$(CC) | | 407 |
| $\nu$(As−C) | 635 | 611 | $\nu$(As−C) | 637 | 627 |
| 4b(a′) | | 708 | 4b(a″) | | 690 |
| $\nu_s$, $\nu_{as}$(As−OH) | 745 | 742 | $\nu_s$, $\nu_{as}$(As−OH) | 744 | |
| $\nu_s(AsO_x)$ | 810 | 795 | $\nu_s(AsO_x)$ | 824 | 797 |
| $\nu_{as}(AsO_x)$ | 855 | 834 | $\nu_{as}(AsO_x)$ | 844 | 813 |
| $NH_2$ | | 983 | $\nu$(CN) | | 1146 |
| 18(a′) | | 1002 | $\nu_s(NO_2)$ | 1342 | 1322 |
| 7(a′) | 1097 | 1089 | $\nu_{as}(NO_x)$ | 1533 | 1490 |
| 9a(a′) | 1183 | 1182 | $\nu$(CC) | 1573 | |
| 19b(b″), $\nu$(CC) + $\delta$(C−H) | | 1448 | $\nu_s$(As═O), $\nu_s(As(OH)O_2^-)$ | | 1591 |
| $\nu_s$(As═O), $\nu_s(As(OH)O_2^-)$ | | 1593 | 8a(a′), 8b(a′), $\nu_{as}(NO_2)$ | 1617 | |

wave (PAW) method[30] was used to describe the interaction between valence electrons and the ionic cores as implemented in VASP code.[31,32] We use PAW potentials with the following valence configurations: $Ag(4d^{10}5s^1)$, $As(4s^24p^3)$, $C(2s^22p^2)$, $H(1s^1)$, $N(2s^22p^3)$, and $O(2s^22p^4)$.

The total-energy calculations were performed using a plane wave basis set with cutoff energy of 470 eV and a convergence tolerance of $1 \times 10^{-6}$ eV. For ionic relaxations, the structures were optimized until the forces on each atom were smaller than 0.01 eV $Å^{-1}$. We constructed a Ag(111) slab based on the calculated equilibrium lattice parameter of bulk Ag, considering that the (111) is the most stable surface.[33]

The slab consists of a $5 \times 5$ repetition of the (111) surface unit cell, and is composed by five layers, where the two bottom layers were frozen and the three topmost layers were allowed to relax. A vacuum region of 2.0 nm was used to separate two neighboring slabs in the $z$ direction, considering that the length of *p*AsA is shorter than 7.3 Å. Integrations over the Brillouin zone were performed using a $2 \times 2 \times 1$ Γ-centered mesh of special $k$ points.

We explored different surface adsorption sites and molecule orientations. For $pAsA^-$ and $pAsA^{2-}$ two molecular orientations were considered: (1) the molecule with its long axis perpendicular to the Ag surface (straight configuration); (2) the molecule long axis forming an acute angle with the Ag surface (tilted configuration). In both cases, the O in the base of the molecule can bind to the Ag surface in three different configurations: (A) O on the top site, i.e., with the O atom located on the top of a Ag atom; (B) O on the bridge site, where the O atom is located in the middle of two neighboring Ag atoms in the same layer (in the middle of the Ag−Ag bond); and (C) O on a hollow site, at the center of a triangle formed by three neighboring Ag atoms. These configurations are shown in Figure S1 in the Supporting Information.

## RESULTS AND DISCUSSION

**Quantitative SERS Studies of Arsenic.** Normal Raman spectra of the arsenic chemicals were collected for reference purposes. Figure S2 shows the normal Raman spectra of the arsenic species studied in this work and their corresponding molecular structures. The SERS spectra for Rox as a function of concentration are shown in Figure 1. The tentatively assigned Raman modes and observed peak frequencies for *p*AsA and Rox for both the normal Raman spectra and the SERS spectra are summarized in Table 1.



DOI: 10.1021/acs.jpca.8b09104
J. Phys. Chem. A 2018, 122, 9474−9482

In the normal Raman spectrum of Rox, the peak frequencies of the symmetric and the asymmetric stretching modes for $AsO_x$ are found at 824 and 844 $cm^{-1}$ respectively. A weak band attributable to an As−OH vibration is found at 744 $cm^{-1}$, and assigned to an As−O stretching for As−OH. An As−C stretching vibration is found at 637 $cm^{-1}$. In the SERS spectrum of Rox, the symmetric and the asymmetric stretching modes of $AsO_x$ shift to lower wavenumbers, 797 and 813 $cm^{-1}$ respectively, which suggests a covalent chemical interaction of As−O with the silver surface forming the As−O−Ag bonds. Supporting evidence for complexation of As−O with the silver surface comes from the observation of a band near 200 $cm^{-1}$, which is attributed to Ag−O stretching. In addition, the stretching mode of As−C is strongly enhanced in the SERS spectrum and shifts by 10 $cm^{-1}$ to lower frequency at 627 $cm^{-1}$. The above changes of the arsenic involved Raman modes can be also observed by comparing the normal Raman spectrum of *p*AsA with its SERS spectrum. Similarly, the symmetric and the asymmetric stretching modes of AsOx in *p*AsA shift from 855 and 810 $cm^{-1}$ to 834 and 795 $cm^{-1}$, respectively, after adsorption onto the silver surface. In addition, the As−C stretching mode shifts from 635 to 611 $cm^{-1}$. Thus, the SERS features of the arsonic acid group are very good identifiers to confirm the presence of organic arsenic species. A broad shoulder assignable to $NH_2$ at 983 $cm^{-1}$ originating from *p*AsA and an intense stretching mode of $NO_2$ at 1322 $cm^{-1}$ found in Rox are specific markers to further distinguish them in the spectrum of mixed organic arsenic species (Figure S3). Interestingly, the peak position of the As−C stretching vibration in the mixture of *p*AsA and Rox is at 623 $cm^{-1}$, which is in between the As−C stretching peaks of pure *p*AsA at 611 $cm^{-1}$ and pure Rox at 628 $cm^{-1}$, reflecting a spectral combination of *p*AsA and Rox.

SERS intensities of Rox at 405, 627, 813, and 1322 $cm^{-1}$ for decreasing concentrations are shown in Figure 1A. Peaks assigned to the As−C stretching at 627 $cm^{-1}$, the asymmetric stretching of $AsO_x$ at 813 $cm^{-1}$, the stretching of $NO_2$ at 1322 $cm^{-1}$, and the asymmetric stretching modes of As═O and $As(OH)O_2^-$ at 1593 $cm^{-1}$ are readily detectable at the lowest concentration, $5 \times 10^{-8}$ M (~3.8 ppb). The result illustrates the high sensitivity of this Ag/AuNRs−PCL SERS substrate for the detection of arsenic with an LOD much lower than the WHO standard of 10 ppb. As all the intensities in the Rox SERS spectrum are decreasing as concentration decreases, no specific peak can be used as an independent reference for normalization and quantification. Due to the excellent reproducibility of the SERS substrate, the background of a bare SERS substrate can be consistently measured and subtracted from SERS spectra of analytes, which results in better quality spectra for quantification. As Figure 1B shows, after spectral processing, all the major peaks of Rox are quantitatively changing as a logarithmic function of concentration, which is consistent with a Langmuir adsorption model.

To test the robustness of the SERS substrate and study the effects of salt ions on the SERS sensitivity for arsenic detection, quantitative SERS measurements of $As^V$ in both DI water and common salt ionic solutions were carried out. SERS spectra of $As^V$ are shown in Figure 2, where the peak at 785 $cm^{-1}$ is assigned to $\nu_1(A_1)$ symmetric As−O stretching. The minor peak around 425 $cm^{-1}$ is the superposition of $\nu_2(A_1)$ and $\nu_5(E)$ stretching modes.[16] The shoulder at 825 $cm^{-1}$ is tentatively assigned to the asymmetric stretching of As−O. As shown in Figure 2B, the salt ions perturbed the SERS detection of $As^V$ to some degree, but an LOD of $10^{-7}$ M (~8 ppb) is still possible. The reduction in SERS signal stems either from salt ion complexation with $AsO_4^{3-}$ during adsorption, or by contamination of the silver surface sites. Cations like $Mg^{2+}$ and $Ca^{2+}$, for example, compete for attachment to the silver surface, to form $Mg_3(AsO_4)_2$ and $Ca_3(AsO_4)_2$ thus reducing the free $As^V$ that can adsorb onto the silver surface.[19] On the other hand, anions like $Cl^-$ and $PO_4^{3-}$ can compete with $AsO_4^{3-}$ to complex with silver and form AgCl and $Ag_3PO_4$, reducing the number of effective sites on the silver surface for $As^V$ adsorption. This interference can lead to poor adsorption efficiency of $As^V$, which eventually results in a lower SERS sensitivity for $As^V$ detection. To avoid complexation by inorganic salt ions in hard water, some preprocessing of samples might be required, such as adding $F^-$ to form precipitates with $Mg^{2+}$ and $Ca^{2+}$, which could then facilitate the SERS performance for arsenate detection.[15]

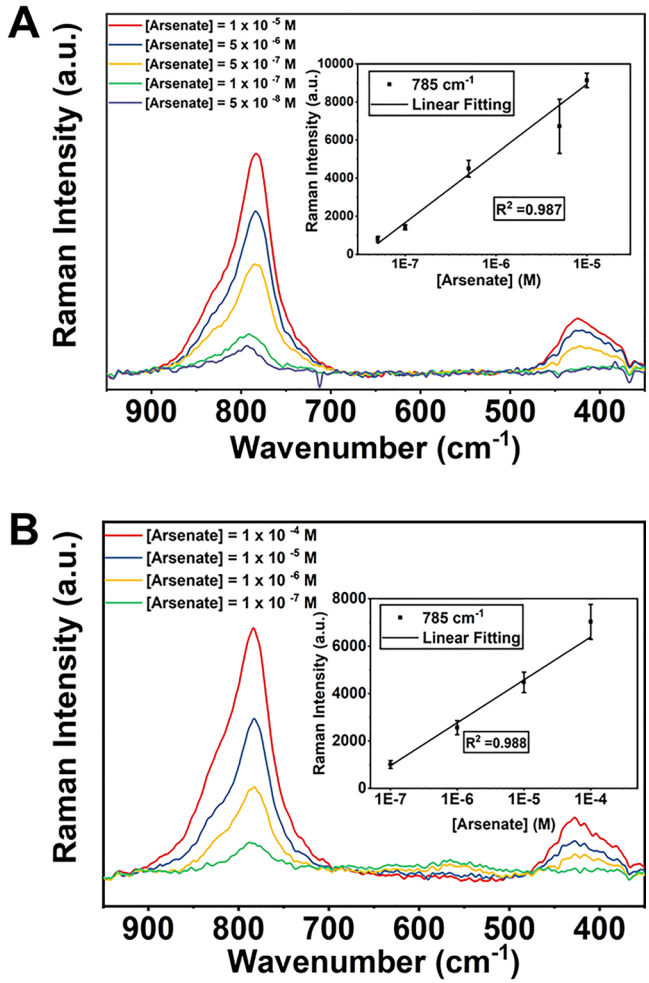


**Figure 2.** (A) SERS spectra of $As^V$ at concentrations ranging from $10^{-5}$ to $5 \times 10^{-8}$ M in DI water. (B) SERS spectra of $As^V$ at concentrations ranging from $10^{-5}$ to $10^{-7}$ M prepared in common salt ion solutions (30 $\mu$M $Na^+$,10 $\mu$M $K^+$, 10 $\mu$M $Mg^{2+}$, 10 $\mu$M $Ca^{2+}$, 10 $\mu$M $Cl^-$, 10 $\mu$M $HPO_4^{2-}$, 10 $\mu$M $SO_4^{2-}$, 20 $\mu$M $NO_3^-$, 10 $\mu$M $H_2PO_4^-$). Inset: SERS intensity at peak 785 $cm^{-1}$ as a function of $As^V$ concentration.

**SERS Analysis of *p*AsA.** When the relationship of the SERS intensity of *p*AsA to its concentration was first studied over the range $5 \times 10^{-8}$−$5 \times 10^{-5}$ M, a low LOD and good quantification were achieved. (Figure 3A,B). At higher


DOI: 10.1021/acs.jpca.8b09104
J. Phys. Chem. A 2018, 122, 9474−9482

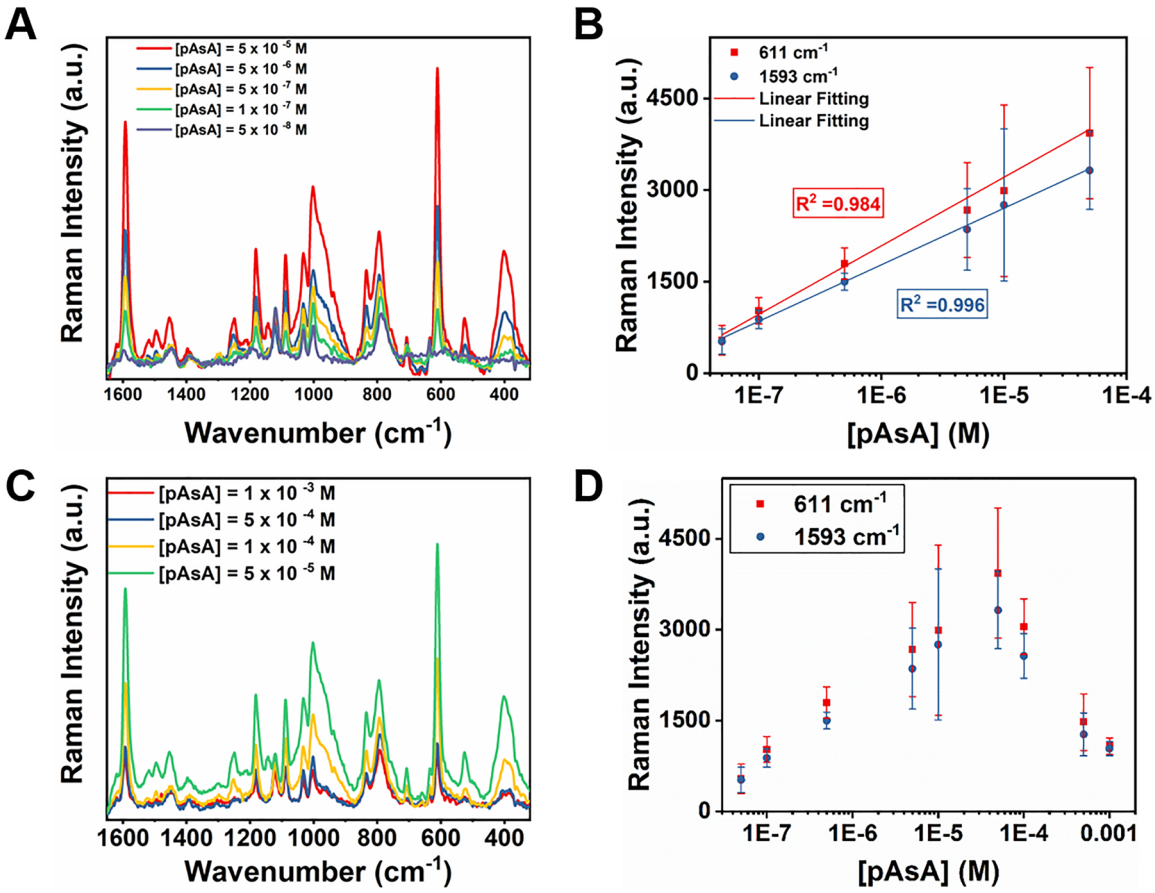


**Figure 3.** (A) SERS spectra of *p*AsA with concentrations ranging from $5 \times 10^{-8}$ to $5 \times 10^{-5}$ M. (B) SERS quantification of *p*AsA against concentration for peaks at 611 and 1593 $cm^{-1}$. (C) SERS spectra of *p*AsA with concentrations ranging from $5 \times 10^{-5}$ to $1 \times 10^{-3}$ M. (D) SERS intensities of *p*AsA for peaks at 611 and 1593 $cm^{-1}$, with the whole concentration range from $5 \times 10^{-8}$ to $1 \times 10^{-3}$ M.

concentrations up to $1 \times 10^{-3}$ M, however, shown in Figure 3C, the SERS intensities of *p*AsA continued to decrease. The maximum of the SERS intensity of *p*AsA occurred approximately at $5 \times 10^{-5}$ M, and the SERS intensity at $1 \times 10^{-3}$ M is comparable to the SERS intensity obtained at $1 \times 10^{-7}$ M as shown in Figure 3D. Although good quantification was obtained at concentrations below $5 \times 10^{-5}$ M, the decreased Raman intensity at higher concentrations of *p*AsA was unexpected. As more and more sites on the surface are occupied, the Raman intensity should approach a limiting value as the surface becomes saturated, which was observed for 4-mercaptopyridine (4-Mpy) in our previous study.[35]

To elucidate the unexpected behavior of intensity with increasing concentration for *p*AsA, we considered the possible molecular structures of *p*AsA in detail. As a polyprotic acid, *p*AsA has three different $pK_a$ values ($pK_{a1} = 1.9$, $pK_{a2} = 4.1$, and $pK_{a3} = 9.2$), and several tautomers can coexist in aqueous solution.[36] With increasing pH, the dominant form of *p*AsA in water changes from protonated *p*AsA, denoted as $pAsA^+$, to neutral *p*AsA, and upon a further increase in pH, it changes to deprotonated *p*AsA, denoted as $pAsA^-$ and $pAsA^{2-}$, as shown in Scheme 1. Using the known values of $pK_a$, one can calculate the equilibrium fraction of each *p*AsA species as a function of pH, since the molar percent of the different arsenic species existing in water is only related to pH.[37] Therefore, the population of different tautomers of *p*AsA can be determined and plotted at every specific pH as shown in Figure S4. At concentrations above $5 \times 10^{-4}$ M, the pH of the *p*AsA solution

**Scheme 1. Different Tautomers of *p*AsA That Can Exist in Water**

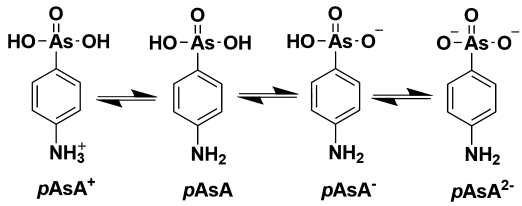


is below 3.9. Figure S4 shows the dominant species in the solution are $pAsA^+$ and *p*AsA. As previously discussed, *p*AsA molecules anchor to the silver surface via As−O−Ag binding, and neither $pAsA^+$ nor *p*AsA can significantly adsorb onto the silver surface. As the concentration of *p*AsA decreases, the pH rises to above 6. More *p*AsA molecules are now in the deprotonated forms, $pAsA^-$ and $pAsA^{2-}$, which are more inclined to interact with the silver surface via the negatively charged As−$O^-$.

To confirm the predominance of the deprotonated forms of *p*AsA rather than the protonated or the neutral *p*AsA in terms of adsorption and SERS activities, a higher concentration of *p*AsA at $5 \times 10^{-4}$ M was chosen for further study under different pH conditions. Various small amounts of 0.1 M NaOH were added to $5 \times 10^{-4}$ M *p*AsA to increase the pH of the solution from 3.90 (no NaOH added) to 4.81 (50 $\mu$L NaOH added). The resultant SERS signal shows a gradual



DOI: 10.1021/acs.jpca.8b09104
J. Phys. Chem. A 2018, 122, 9474−9482

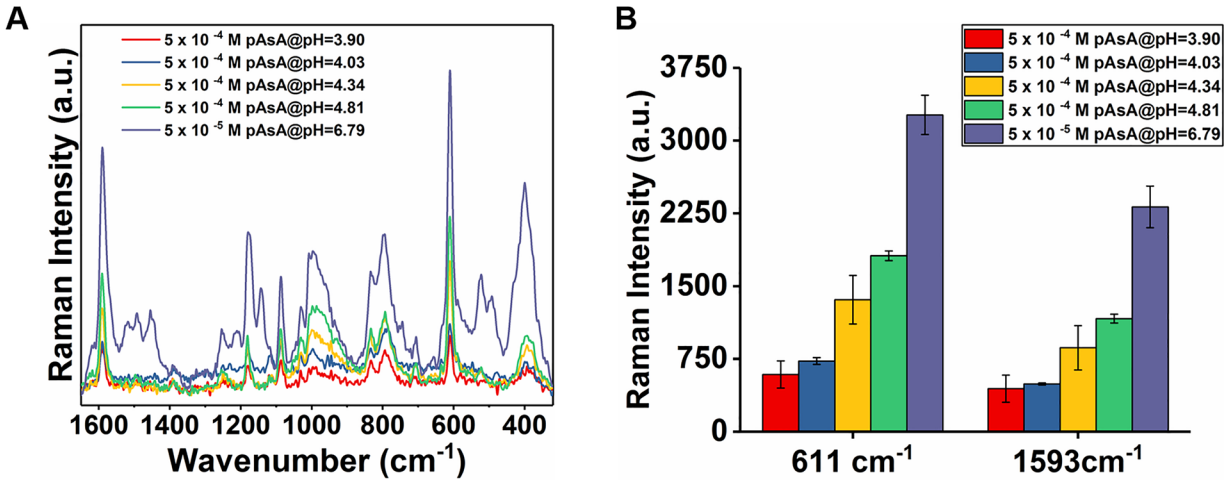


**Figure 4.** (A) SERS spectra of $5 \times 10^{-4}$ M *p*AsA under different pH conditions and $5 \times 10^{-5}$ M *p*AsA (no NaOH added). (B) SERS intensity comparison of the 611 and 1593 $cm^{-1}$ peaks of *p*AsA at $5 \times 10^{-4}$ M at different pH values and *p*AsA at $5 \times 10^{-5}$ M (no NaOH added).

increase in intensity as shown in Figure 4. This proves that the SERS intensities of *p*AsA are truly related to its tautomer population. It should also be noted that no higher pH of the *p*AsA was obtained in this study, since the amount of NaOH was calculated to ensure the pH value is totally contributed by the tautomers of *p*AsA and not the extra $OH^-$ from NaOH left in the solution. In other words, for the highest pH value of 4.81 obtained in this case, the amount of NaOH added into the solution turned all *p*AsA in the solution into $pAsA^-Na^+$ salt as an initial solute.

Interestingly, for the SERS intensities of $5 \times 10^{-4}$ M *p*AsA obtained at different pH values compared to the SERS intensity of $5 \times 10^{-5}$ M, the SERS intensities obtained at the former were still much weaker than the SERS intensity obtained at the latter, which has a pH of approximately 6.79. In addition, there are two deprotonated tautomers of *p*AsA: $pAsA^-$ and $pAsA^{2-}$. The roles these two tautomers play in the *p*AsA adsorption and SERS response require further elucidation. The concentrations of different *p*AsA tautomers calculated from the solution concentration and pH values are shown in Table S1. $[pAsA^-]$ species existing in $5 \times 10^{-4}$ M solutions under different pH conditions were all about an order of magnitude higher than $[pAsA^-]$ existing in $5 \times 10^{-5}$ M solution. This trend is opposite to the observed trend of SERS intensities, as shown in Figure 4B. This result suggests that the $pAsA^-$ was not the predominant tautomer giving rise to SERS intensities. $[pAsA^{2-}]$ is the species responsible for the SERS intensities, which changed from 1 to 17 nM with pH increasing from 3.90 to 4.81 while reaching the highest at approximately 200 nM in $5 \times 10^{-5}$ M solution; that is consistent with the change of SERS intensities. Moreover, the SERS intensities, for instance, peaks 611 and 1593 $cm^{-1}$, which are assigned to As−C stretching and combination of As═O and $As(OH)O_2^-$, respectively, exhibited a linear relationship between the Raman intensity and the logarithmic function of $[pAsA^{2-}]$, as shown in Figure 5. Thus, $pAsA^{2-}$, we believe, is the tautomer that contributes most of the SERS intensity even though a very trace amount of $pAsA^{2-}$ (nanomolar level) exists in the *p*AsA solutions.

The coexistence of both bidentate and monodentate adsorption structures of the monophenyl substituted organo-arsenic species adsorbed on ferrihydrite has been suggested by an EXAFS study.[38] The structure of the bound *p*AsA has been

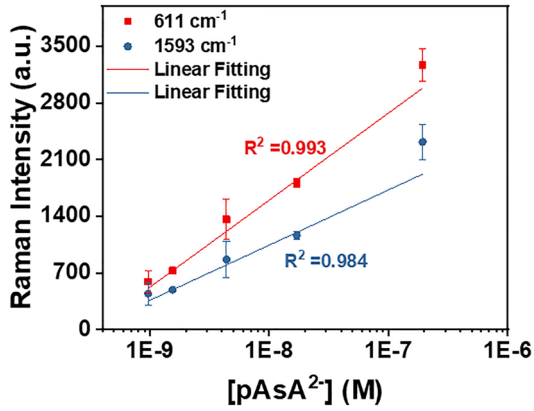


**Figure 5.** SERS intensity of *p*AsA peaks at 611 and 1593 $cm^{-1}$ plotted against concentration of $pAsA^{2-}$.

calculated for both monodentate and bidentate adsorption structures that can complex with hydrated iron oxide clusters to form outer- and inner-sphere complexes based on DFT.[8] In our study, DFT calculations of $pAsA^-$ and $pAsA^{2-}$ interacting with Ag surface have been executed to elucidate the spectral observation of *p*AsA discussed above. The computational results for $pAsA^-$ and $pAsA^{2-}$ on the Ag(111) surface indicate that the bottom O atom binds to the surface on the bridge site, with two different orientations. The monodentate structure is energetically more favorable for $pAsA^-$ in a tilted configuration, which is 151 meV lower in energy than the straight configuration, as shown in Figure 6. The phenyl group of $pAsA^-$ forms an angle of 44° with the surface plane. In contrast, the deprotonated species $pAsA^{2-}$ tends to adsorb in a straight configuration; i.e., the phenyl group is almost perpendicular to the surface, forming an angle of 85° with the surface plane. We find that, starting with a tilted configuration, the $pAsA^{2-}$ spontaneously relaxes to the straight configuration. Thus, the slight energy difference of $pAsA^{2-}$ on the bridge site for straight (0.00 meV) and tilted (1.33 meV) configurations is due to the similar final optimized structures. The total energy differences between the various configurations tested are listed in Table S2 in the Supporting Information.



DOI: 10.1021/acs.jpca.8b09104
J. Phys. Chem. A 2018, 122, 9474−9482

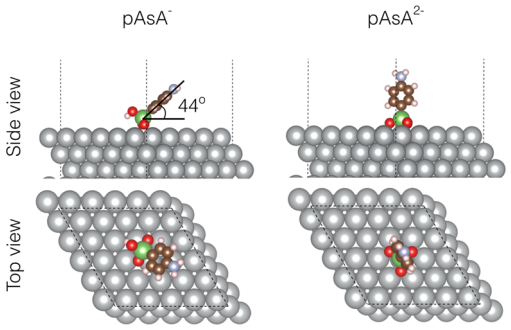


**Figure 6.** Optimized $pAsA^{-}$ and $pAsA^{2-}$ on the Ag(111) surface. Both molecules tend to adsorb on the bridge site (see Figure S1), yet with different inclinations. H, O, N, C, As, and Ag are represented by pink, red, blue, brown, green, and gray spheres, respectively.

The different orientations of the adsorbed $pAsA^{-}$ (tilted) and $pAsA^{2-}$ (straight) on the Ag(111) surface are expected to result in large differences in their contributions to the observed SERS intensities. When $pAsA^{2-}$ is bound to the silver surface, the orientation of the phenyl group is perpendicular to the surface. The polarizability change of the phenyl breathing vibrational mode is also perpendicular to the silver surface, and results in a high SERS signal as suggested by the SERS selection rules.[39] When the phenyl group is instead tipped away from the surface normal, there is less coupling to the SERS electromagnetic field localized around silver surface and this results in a much weaker SERS signal, even though $pAsA^{-}$ could be the major species adsorbed on the silver surface. Interestingly, the different binding orientations of $pAsA^{-}$ and $pAsA^{2-}$ to the silver surface lead to little changes in peak positions, but large changes in peak intensities. This suggests that the changes in the orientation angles do not always cause considerable changes in Raman frequency.[40] In our case, the lack of peak shifts between $pAsA^{-}$ and $pAsA^{2-}$ could be due to (1) the bulky $AsO_3$− group attached on the surface which prevents the phenyl group from further approaching and contacting the silver surface and (2) the para functional group $-NH_2$ that cannot effectively interact with the silver surface. This resulted in little change in peak position with only an intensity change between $pAsA^{2-}$ and $pAsA^{-}$.

**In Situ SERS of Arsenic Activities.** In addition to quantification and speciation of arsenic, the Ag/AuNRs−PCL SERS substrate also serves as a platform for in situ observation of changes in arsenic activities, such as $As^{V}$ desorption and Rox reduction, as shown in Figure 7.

As for in situ desorption of $As^{V}$, different desorbing agents $KH_2PO_4$ and NaCl were used to compare the desorption efficiency. As seen in the inset in Figure 7A, $H_2PO_4^{-}$ desorbed $As^{V}$ from the SERS substrate more efficiently than $Cl^{-}$. More than 80% of the $As^{V}$ was removed from the substrate by $H_2PO_4^{-}$ within 30 min, while only about 50% of the $As^{V}$ desorbed from the substrate in the $Cl^{-}$ case after a 90 min desorption. As for in situ reduction of Rox by $NaBH_4$ shown in Figure 7B, the $NO_2$ symmetric stretching vibration, $\nu_s(NO_2)$, at 1322 $cm^{-1}$ quickly disappeared within 1 min. In addition, a new peak at 983 $cm^{-1}$, assigned to $NH_2$, showed a gradual increase in intensity with time indicating reduction of the $NO_2$ by $NaBH_4$ accompanied by the formation of $NH_2$.

## CONCLUSION

These results describe the first successful speciation and quantification of the different arsenic species using a Ag/AuNR decorated 3D polymer SERS substrate. They demonstrate an LOD of 4 ppb in DI water and 8 ppb in common salt ionic solutions. Moreover, these SERS substrates have shown the versatility to investigate in situ SERS monitoring of arsenic desorption and reduction, providing an excellent sensing platform for both fundamental and applied studies. Significantly, a detailed analysis of the SERS spectra of *p*AsA provided insightful information on the nature of the binding structures of *p*AsA onto the silver surface. We were able to then draw the conclusion that $pAsA^{-}$ and $pAsA^{2-}$ are the *p*AsA tautomers that can effectively be adsorbed onto the silver surface via formation of As−O−Ag bonds. We also concluded that $pAsA^{2-}$ is the tautomer that contributes the most SERS intensity due to its orientation and chemical interaction with the silver surface. These results were corroborated by DFT calculations for the bonding configurations of $pAsA^{-}$ and $pAsA^{2-}$ on the Ag(111) surface. All the results have explicitly indicated that this 3D Ag/AuNRs−PCL SERS substrate is of great potential for use as an environmental sensor for arsenic analysis.

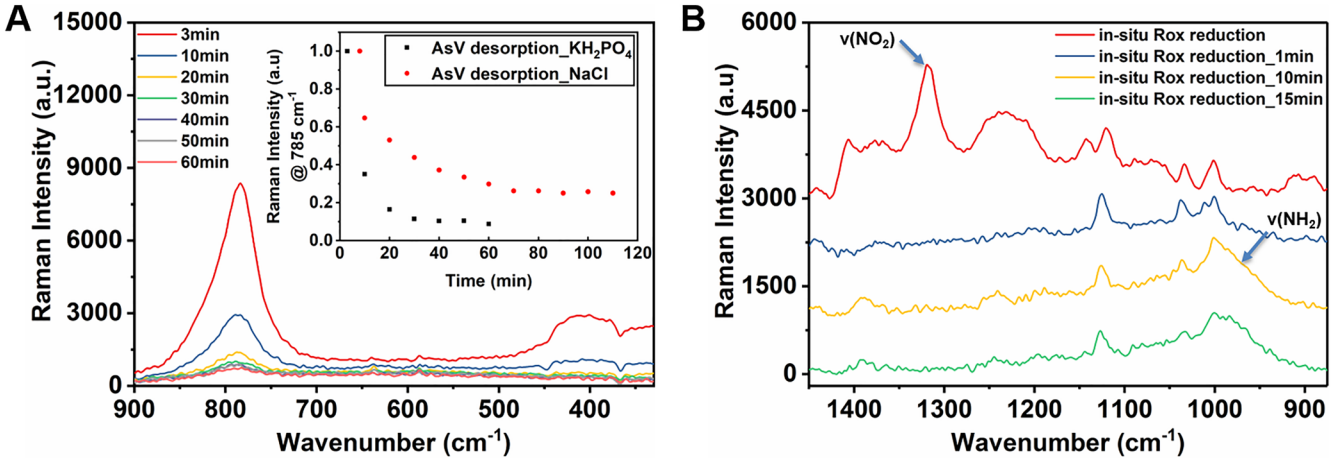


**Figure 7.** (A) In situ SERS spectra of $As^{V}$ desorption at a concentration of $10^{-4}$ M in 20 mg/L $KH_2PO_4$. Inset: Normlized Raman intensity of 785 $cm^{-1}$ peak of $As^{V}$ as a function of time illustrating its desorption in 20 mg/L $KH_2PO_4$ and NaCl, respectively. (B) In situ SERS spectra of $5 \times 10^{-5}$ M Rox reduction with time in 2 mM $NaBH_4$.



DOI: 10.1021/acs.jpca.8b09104
J. Phys. Chem. A 2018, 122, 9474−9482

## ■ ASSOCIATED CONTENT

### Supporting Information

The Supporting Information is available free of charge on the ACS Publications website at DOI: 10.1021/acs.jpca.8b09104.

Possible adsorption sites of $p$AsA$^{-}$ and $p$AsA$^{2-}$ on a silver surface; normal Raman spectra of arsenic species; SERS spectra of $p$AsA/Rox mixture and As$^{III}$/As$^{V}$ mixture; $p$AsA polyprotic distribution as a function of pH; population of different tautomers in $p$AsA solution under different pHs; total energy differences for $p$AsA$^{-}$ and $p$AsA$^{2-}$ in different adsorption sites and molecule orientations; in situ SERS of $10^{-4}$ M As$^{V}$ desorption in 20 mg/L NaCl solution (PDF)

## ■ AUTHOR INFORMATION


### Corresponding Author

*E-mail: rabolt@udel.edu. Fax: 302-831-4545. Tel.: 302-831-4476.

### ORCID

John F. Rabolt: 0000-0003-4132-4266



### Funding

The authors would like to acknowledge the support from Delaware NSF EPSCoR Grant 1301765 and the NSF DMR Polymers Program Grant DMR-1407255. A.J. and F.P.S. were supported by the National Science Foundation Grant DMR-1652994. The calculations were performed using the Extreme Science and Engineering Discovery Environment supercomputer facility, National Science Foundation Grant ACI-1053575.


### Notes

The authors declare no competing financial interest.

## ■ REFERENCES


(1) Mohan, D.; Pittman, C. U. Arsenic Removal from Water/Wastewater Using Adsorbents—a Critical Review. *J. Hazard. Mater.* **2007**, *142*, 1−53.

(2) Ravenscroft, P.; Brammer, H.; Richards, K. *Arsenic Pollution: A Global Synthesis*; John Wiley & Sons: Chichester, U.K., 2009.

(3) Abhyankar, L. N.; Jones, M. R.; Guallar, E.; Navas-Acien, A. Arsenic Exposure and Hypertension: A Systematic Review. *Environ. Health Perspect.* **2012**, *120*, 494−500.

(4) Hao, J.; Han, M.-J.; Han, S.; Meng, X.; Su, T.-L.; Wang, Q. K. Sers Detection of Arsenic in Water: A Review. *J. Environ. Sci.* **2015**, *36*, 152−162.

(5) Wu, Y.; Zhan, S.; Wang, F.; He, L.; Zhi, W.; Zhou, P. Cationic Polymers and Aptamers Mediated Aggregation of Gold Nanoparticles for the Colorimetric Detection of Arsenic(Iii) in Aqueous Solution. *Chem. Commun.* **2012**, *48*, 4459.

(6) Jones, F. T. A Broad View of Arsenic. *Poult. Sci.* **2007**, *86*, 2−14.

(7) Makris, K. C.; Quazi, S.; Punamiya, P.; Sarkar, D.; Datta, R. Fate of Arsenic in Swine Waste from Concentrated Animal Feeding Operations. *J. Environ. Qual.* **2008**, *37*, 1626−1633.

(8) Adamescu, A.; Hamilton, I. P.; Al-Abadleh, H. A. Density Functional Theory Calculations on the Complexation of P-Arsanilic Acid with Hydrated Iron Oxide Clusters: Structures, Reaction Energies, and Transition States. *J. Phys. Chem. A* **2014**, *118*, 5667−5679.

(9) Gómez-Ariza, J. L.; Sánchez-Rodas, D.; Giráldez, I.; Morales, E. A Comparison between Icp-Ms and Afs Detection for Arsenic Speciation in Environmental Samples. *Talanta* **2000**, *51*, 257−268.

(10) Sheppard, B. S.; Caruso, J. A.; Heitkemper, D. T.; Wolnik, K. A. Arsenic Speciation by Ion Chromatography with Inductively Coupled Plasma Mass Spectrometric Detection. *Analyst* **1992**, *117*, 971−975.

(11) Mattusch, J.; Wennrich, R. Determination of Anionic, Neutral, and Cationic Species of Arsenic by Ion Chromatography with Icpms Detection in Environmental Samples. *Anal. Chem.* **1998**, *70*, 3649−3655.

(12) Jackson, B. P.; Bertsch, P. M. Determination of Arsenic Speciation in Poultry Wastes by Ic-Icp-Ms. *Environ. Sci. Technol.* **2001**, *35*, 4868−4873.

(13) Halvorson, R. A.; Vikesland, P. J. Surface-Enhanced Raman Spectroscopy (Sers) for Environmental Analyses. *Environ. Sci. Technol.* **2010**, *44*, 7749−7755.

(14) Alvarez-Puebla, R. A.; Liz-Marzan, L. M. Environmental Applications of Plasmon Assisted Raman Scattering. *Energy Environ. Sci.* **2010**, *3*, 1011−1017.

(15) Xu, Z. H.; Jing, C. Y.; Hao, J. M.; Christodoulatos, C.; Korfiatis, G. P.; Li, F. S.; Meng, X. G. Effect of Bonding Interactions between Arsenate and Silver Nanofilm on Surface-Enhanced Raman Scattering Sensitivity. *J. Phys. Chem. C* **2012**, *116*, 325−329.

(16) Mulvihill, M.; Tao, A.; Benjauthrit, K.; Arnold, J.; Yang, P. Surface-Enhanced Raman Spectroscopy for Trace Arsenic Detection in Contaminated Water. *Angew. Chem., Int. Ed.* **2008**, *47*, 6456−6460.

(17) Li, J.; Chen, L.; Lou, T.; Wang, Y. Highly Sensitive Sers Detection of As3+ Ions in Aqueous Media Using Glutathione Functionalized Silver Nanoparticles. *ACS Appl. Mater. Interfaces* **2011**, *3*, 3936−3941.

(18) Du, J. J.; Cui, J. L.; Jing, C. Y. Rapid in Situ Identification of Arsenic Species Using a Portable Fe3o4@Ag Sers Sensor. *Chem. Commun.* **2014**, *50*, 347−349.

(19) Xu, Z. H.; Hao, J. M.; Li, F. S.; Meng, X. G. Surface-Enhanced Raman Spectroscopy of Arsenate and Arsenite Using Ag Nanofilm Prepared by Modified Mirror Reaction. *J. Colloid Interface Sci.* **2010**, *347*, 90−95.

(20) Hao, J. M.; Han, M. J.; Xu, Z. H.; Li, J. W.; Meng, X. G. Fabrication and Evolution of Multilayer Silver Nanofilms for Surface-Enhanced Raman Scattering Sensing of Arsenate. *Nanoscale Res. Lett.* **2011**, *6*, 263.

(21) Xu, Z. H.; Meng, X. G.; Zhang, Y. J.; Li, F. S. Effects and Mechanisms of Water Matrix on Surface-Enhanced Raman Scattering Analysis of Arsenite on Silver Nanofilm. *Colloids Surf., A* **2016**, *497*, 117−125.

(22) Chen, C. F.; Hao, J. M.; Zhu, L. Y.; Yao, Y. Q.; Meng, X. G.; Weimer, W. N.; Wang, Q. W. K. Direct Two-Phase Interfacial Self-Assembly of Aligned Silver Nanowire Films for Surface Enhanced Raman Scattering Applications. *J. Mater. Chem. A* **2013**, *1*, 13496−13501.

(23) Xu, S.; Tang, W.; Chase, D. B.; Sparks, D. L.; Rabolt, J. F. A Highly Sensitive, Selective, and Reproducible Sers Sensor for Detection of Trace Metalloids in the Environment. *ACS Appl. Nano Mater.* **2018**, *1*, 1257−1264.

(24) Hohenberg, P.; Kohn, W. Inhomogeneous Electron Gas. *Phys. Rev.* **1964**, *136*, B864−B871.

(25) Kohn, W.; Sham, L. J. Self-Consistent Equations Including Exchange and Correlation Effects. *Phys. Rev.* **1965**, *140*, A1133−A1138.

(26) Perdew, J. P.; Burke, K.; Ernzerhof, M. Generalized Gradient Approximation Made Simple. [Phys. Rev. Lett. 77, 3865 (1996)]. *Phys. Rev. Lett.* **1997**, *78*, 1396.

(27) Grimme, S. Accurate Description of Van Der Waals Complexes by Density Functional Theory Including Empirical Corrections. *J. Comput. Chem.* **2004**, *25*, 1463−1473.

(28) Grimme, S.; Antony, J.; Ehrlich, S.; Krieg, H. A Consistent and Accurate Ab Initio Parametrization of Density Functional Dispersion Correction (Dft-D) for the 94 Elements H-Pu. *J. Chem. Phys.* **2010**, *132*, 154104.

(29) Moellmann, J.; Grimme, S. Importance of London Dispersion Effects for the Packing of Molecular Crystals: A Case Study for Intramolecular Stacking in a Bis-Thiophene Derivative. *Phys. Chem. Chem. Phys.* **2010**, *12*, 8500−8504.

(30) Blöchl, P. E. Projector Augmented-Wave Method. *Phys. Rev. B: Condens. Matter Mater. Phys.* **1994**, *50*, 17953−17979.




DOI: 10.1021/acs.jpca.8b09104
J. Phys. Chem. A 2018, 122, 9474−9482

(31) Kresse, G.; Hafner, J. Ab Initio Molecular Dynamics for Open-Shell Transition Metals. *Phys. Rev. B: Condens. Matter Mater. Phys.* **1993**, *48*, 13115−13118.
(32) Kresse, G.; Joubert, D. From Ultrasoft Pseudopotentials to the Projector Augmented-Wave Method. *Phys. Rev. B: Condens. Matter Mater. Phys.* **1999**, *59*, 1758−1775.
(33) Skriver, H. L.; Rosengaard, N. M. Surface Energy and Work Function of Elemental Metals. *Phys. Rev. B: Condens. Matter Mater. Phys.* **1992**, *46*, 7157−7168.
(34) Olavarria-Fullerton, J.; Wells, S.; Ortiz-Rivera, W.; Sepaniak, M. J.; De Jesus, M. A. Surface-Enhanced Raman Scattering (Sers) Characterization of Trace Organoarsenic Antimicrobials Using Silver/Polydimethylsiloxane Nanocomposites. *Appl. Spectrosc.* **2011**, *65*, 423−428.
(35) Tang, W.; Chase, D. B.; Rabolt, J. F. Immobilization of Gold Nanorods onto Electrospun Polycaprolactone Fibers Via Polyelectrolyte Decoration–a 3d Sers Substrate. *Anal. Chem.* **2013**, *85*, 10702−10709.
(36) Depalma, S.; Cowen, S.; Hoang, T.; Al-Abadleh, H. A. Adsorption Thermodynamics of P-Arsanilic Acid on Iron (Oxyhydr)-Oxides: In-Situ Atr-Ftir Studies. *Environ. Sci. Technol.* **2008**, *42*, 1922−1927.
(37) Harvey, D. *Modern Analytical Chemistry*; McGraw-Hill: 2000.
(38) Tanaka, M.; Togo, Y. S.; Yamaguchi, N.; Takahashi, Y. An Exafs Study on the Adsorption Structure of Phenyl-Substituted Organoarsenic Compounds on Ferrihydrite. *J. Colloid Interface Sci.* **2014**, *415*, 13−17.
(39) Moskovits, M.; Suh, J. S. Surface Selection Rules for Surface-Enhanced Raman Spectroscopy: Calculations and Application to the Surface-Enhanced Raman Spectrum of Phthalazine on Silver. *J. Phys. Chem.* **1984**, *88*, 5526−5530.
(40) Smith, W. E. Practical Understanding and Use of Surface Enhanced Raman Scattering/Surface Enhanced Resonance Raman Scattering in Chemical and Biological Analysis. *Chem. Soc. Rev.* **2008**, *37*, 955−964.


DOI: 10.1021/acs.jpca.8b09104
*J. Phys. Chem. A* 2018, 122, 9474−9482